Mechanical, Permeability, and Degradation Properties of 3D Designed Poly(1,8 Octanediol-*co*-Citrate) Scaffolds for Soft Tissue Engineering

Claire G. Jeong,[1] Scott J. Hollister[1,2,3]

[1] Department of Biomedical Engineering, University of Michigan, Ann Arbor 48109-2125, Michigan

[2] Department of Mechanical Engineering, University of Michigan, Ann Arbor 48109-2125, Michigan

[3] Department of Surgery, University of Michigan, Ann Arbor 48109-0329, Michigan

Received 13 January 2009; revised 8 October 2009; accepted 12 October 2009
Published online 20 January 2010 in Wiley InterScience (www.interscience.wiley.com). DOI: 10.1002/jbm.b.31568

Abstract: Poly(1,8-octanediol-*co*-citric acid) (POC) is a synthetic biodegradable elastomer that can be processed into three-dimensional (3D) scaffolds for tissue engineering. We investigated the effect of designed porosity on the mechanical properties, permeability, and degradation profiles of the POC scaffolds. For mechanical properties, scaffold compressive data were fitted to a one-dimensional (1D) nonlinear elastic model, and solid tensile data were fitted to a Neohookean incompressible nonlinear elastic model. Chondrocytes were seeded on scaffolds to assess the biocompatibility of POC. Increased porosity was associated with increased degradation rate, increased permeability, and decreased mechanical stiffness, which also became less nonlinear. Scaffold characterization in this article will provide design guidance for POC scaffolds to meet the mechanical and biological parameters needed for engineering soft tissues such as cartilage. © 2010 Wiley Periodicals, Inc. J Biomed Mater Res Part B: Appl Biomater 93B: 141–149, 2010

Keywords: tissue scaffold; poly(1,8-octanediol-*co*-citrate); elastomer; permeability; degradation

INTRODUCTION

Tissue engineering requires the use of three-dimensional scaffolds as a template on which cells differentiate, proliferate, and grow new tissues. Optimal scaffolds should be biocompatible, biodegradable, permeable, reproducible, noncytotoxic, and capable of serving as a temporary support for the cells with elastic properties similar to native tissue, which will allow eventual replacement by tissue matrix.[1] The choice of scaffold material and architecture will determine the effective scaffold mechanical and mass transport properties that can significantly influence tissue regeneration. Particularly, for cartilage regeneration, many researchers have tried to develop novel materials that are elastomeric yet mechanically tough. Recently, novel elastomeric materials such as poly(1,8-octanediol-*co*-citrate) (POC),[2–5] poly(glycerol sebacate) (PGS),[6–11] and polycaprolactone fumarate (PCLF)[12] have been developed and shown to have potential for soft tissue applications. Among them, POC has been shown to be a good candidate for cartilage tissue engineering[13] because of its biocompatibility, biodegradability, and compressive properties. Cartilage applications require a 3D designed porous architecture with well characterized mechanical and mass transport properties. Even though Kang et al.[13] has shown that POC has potential as a base material for cartilage, the influence of designed POC scaffold porosity on mechanical, mass transport, and degradation properties has not been elucidated.

Scaffold architecture and mechanical and degradation properties are intimately coupled. Scaffold pore architecture in addition to base POC material properties are the two determinants of effective POC scaffold mechanical properties. Furthermore, since POC is mainly degraded by the hydrolysis of its ester linkages,[2,3] scaffold architecture significantly affects scaffold degradation by directing fluid diffusion. To characterize the coupling of architecture and materials with mechanical, mass transport and degradation properties, we fabricated 3D scaffolds with varying porosities, characterizing the resulting mechanical, permeability, and degradation properties of different designs. Scaffold architecture is defined to include pore shape, pore size, and

Correspondence to: S.J. Hollister (e-mail: scottho@umich.edu)
Contract grant sponsor: NIH; Contract grant number: R01 AR 053379

pore interconnectivity. To solely examine the effects of porosity on scaffold property changes in this article, pore shape and pore size were kept constant.

MATERIALS AND METHODS

Synthesis of Prepoly(1,8 Octanediol-*co*-Citrate)

All chemicals were purchased from Sigma-Aldrich (Milwaukee, WI). Poly(1,8 octanediol-*co*-citrate) prepolymer (pPOC) was synthesized following protocols described by Yang et al.[2,3,5], with some curing process modifications. Briefly, equimolar amounts of citric acid and 1,8-octanediol were added to a 500-mL three-necked, round-bottom flask fitted with an inlet and outlet adapter. The mixture was melted at 160–165°C for 15–20 min under a flow of nitrogen gas while stirring. The temperature of the system was subsequently lowered to 140°C for 45 min with constant stirring to create a prepolymer.

Scaffold Design and Fabrication

Previously developed image-based design processes and software were used to design 3D POC scaffold architectures.[5,14–16] Porous POC scaffolds (6.35 mm diameter, 4.0 mm height, 900 μm interconnected cylindrical pores, porosity = 32, 44, and 62%) were designed using custom IDL programs (RSI, Boulder, CO). The details of POC solid and scaffold fabrications were previously reported by Kim et al.[5] In brief, wax molds with 3D-image-based design architecture were built by a Solidscape Patternmaster™ machine and inversely solid free-form fabricated hydroxyapatite (HA) molds were prepared before curing pPOC into architecture scaffolds.[17] Wax molds that embody the designed 3D architecture are fabricated first. However, as the wax molds melt POC curing temperatures, secondary HA were created from the wax molds as the HA easily withstands the pPOC curing temperatures that reach more than 100°C. pPOC was poured into the wells of a Teflon mold, and HA molds were embedded within the pPOC. The pPOC/HA/Teflon mold unit was postpolymerized at 100°C for 1 day followed by curing at 100°C for 3 days more with vacuum (−20 in Hg). The HA mold was removed using a decalcifying reagent (RDO, APEX Engineering Products Corp, Plainfield, IL) followed by incubation in water (Milli-Q water purification system, Billerica, MA) for 24 h to obtain the final porous POC scaffolds (Figure 1). Figure 2 summarizes the complete procedure from design through fabrication and evaluation.

Mechanical Tests

For scaffold unconfined compression tests, seven porous scaffolds from each design were tested in compression (Alliance RT/30 electromechanical test frame, 50 N load cell with 0.5% error range, MTS Systems Corp., MN) and TestWorks4 software (MTS Systems Corp., MN) were used to collect data during compression testing. MATLAB (The MathWorks Inc., MA) software was used to fit a nonlinear elasticity model, $T = A[e^{BE} - 1]$, where T is the first Piola-Kirchoff stress, E is the large strain, and A and B are constants fit to data. Specifically, the sum of least square error between the model and experimental stress was minimized using the LSQNONLIN minimization program in the MATLAB optimization toolbox. Tangent moduli were calculated at 1, 10, 30, and 50% strain from fit data.[18] All residuals between model and experimental stress were below 1%. The compressive Young's modulus of 62% porous scaffolds ($N = 4$, 0.1M NaOH degradation samples) was determined from the initial slope of the stress–strain data (10–20% strain range) obtained from compression tests at a crosshead speed of 2 mm/min. The initial height of each scaffold was measured with an electronic caliper.

To determine if POC exhibited viscoelastic properties, confined compression tests were performed. The same compression test frame as for the unconfined test was used except that the sample was confined by acrylic confined chamber similar to the one described in Refs. [19–23], with a constant chamber temperature of 37°C. A 6.35-mm diameter porous metal indenter was used for compression instead of a regular fixed metal platen. Ten solid cylinders (6.35 mm in diameter, 4.0 mm in height) with the same curing conditions as other scaffolds were tested, and the resulting data were fitted to the nonlinear elastic model.

Tensile mechanical tests were conducted according to ASTM D412a on the same test frame equipped with 500N load cell. Briefly, the dumbbell-shaped sample (33 × 6 × 2.0 mm) was pulled at a rate of 2 mm/s. Assuming POC to be incompressible, the tensile tests were fit to a Neohookean nonlinear elastic model (Holzapfel, G. Nonlinear Solid Mechanics, Wiley; first edition)[24] of the form:

$$W(\lambda_1, \lambda_2, \lambda_3) = \frac{\mu_1}{2}\left(\lambda_1^2 + \lambda_2^2 + \lambda_3^2\right)$$

where W is the strain energy function, λ_i are principal stretch ratios, and μ_1 is a model constant determined by fitting the model to experimental data. The Neohookean model was fit to experimental data by first deriving the first Piola–Kirchoff model stress. The least square error between the model stress and first Piola–Kirchoff experimental stress was minimized using the MATLAB unconstrained minimization function FMINUNC. The Baker-Ericksen inequality (required for physical stability of the model constants) was calculated for each fit and found to be satisfied.

Porosity and Permeability Measurements

Seven scaffolds from each porosity were scanned in air using a MS-130 high-resolution μCT scanner (GE Medical Systems, Toronto, CAN) at 19 μm voxel resolution, at 75 kV and 75 mA. The porosity of each specimen was calculated by defining a region of interest that encompassed the entire scaffold and an appropriate threshold level was

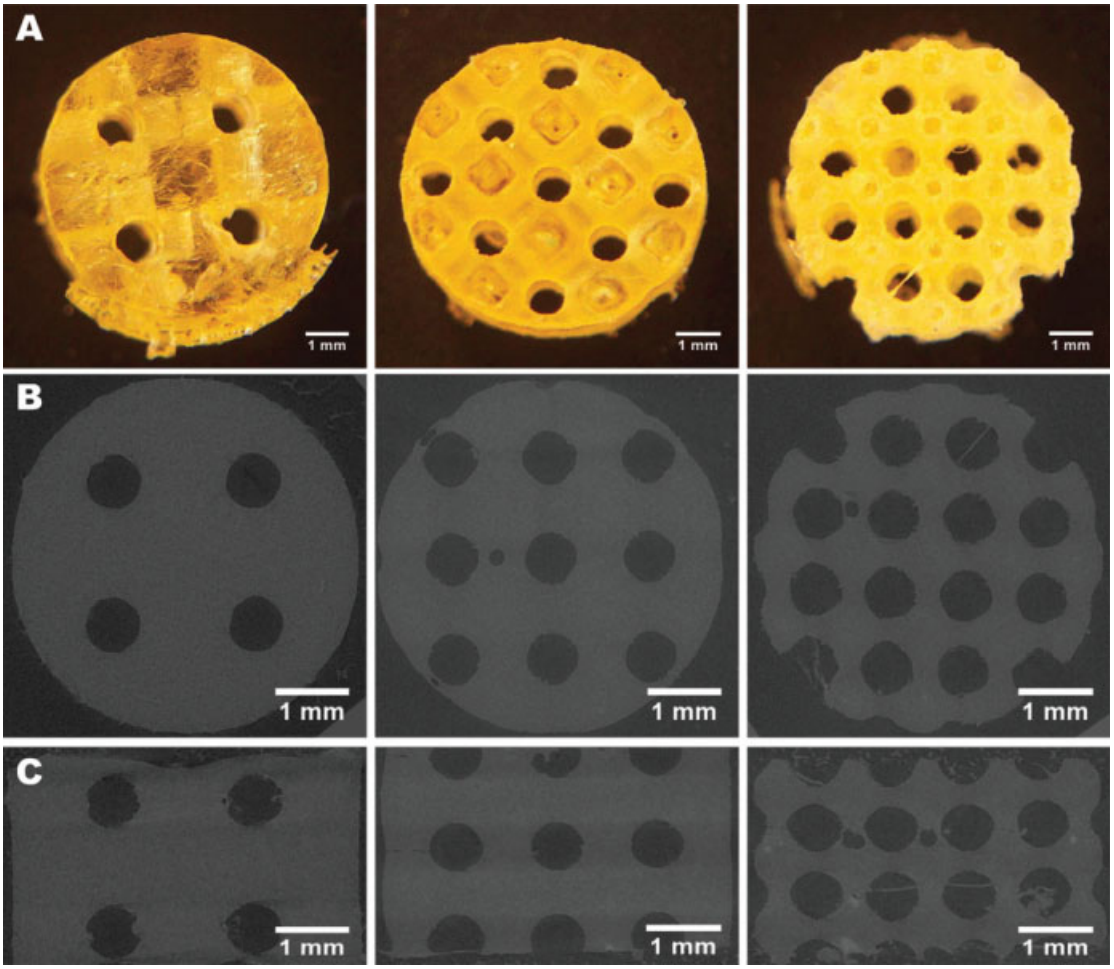

Figure 1. 3D-designed POC scaffolds illustrated through digital images, top view (A) and microCT images, top view (B) and side view (C). [Color figure can be viewed in the online issue, which is available at www.interscience.wiley.com.]

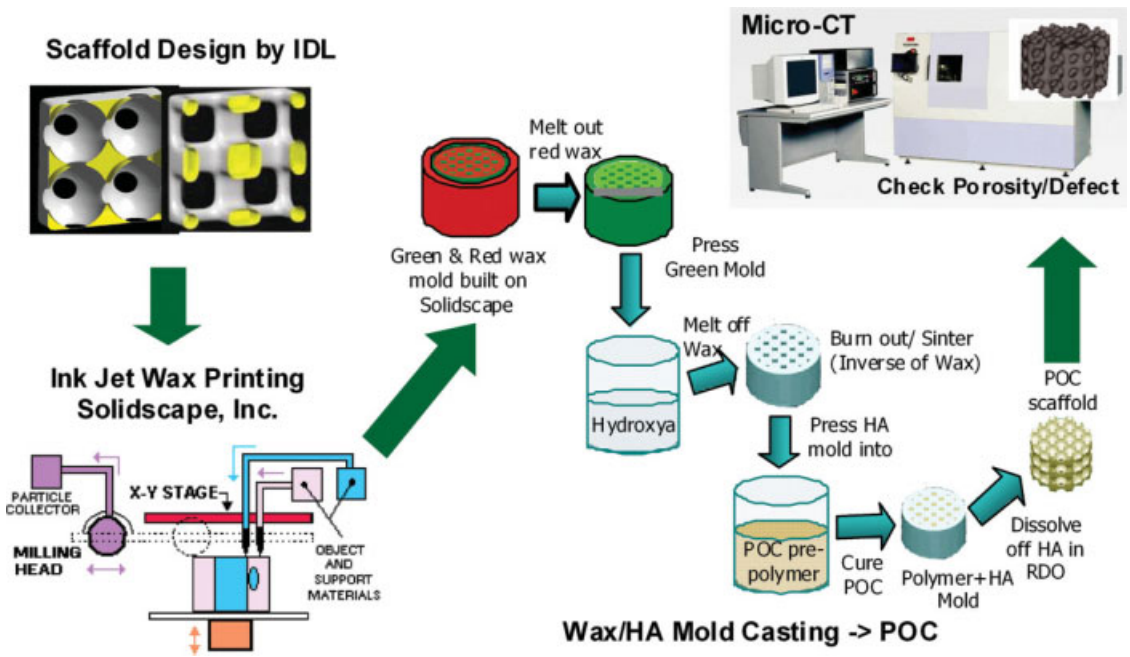

Figure 2. A schematic of designing, fabrication, and porosity analysis of 3D POC scaffolds: with 3D scaffold designs by IDL, first wax molds are built in Solidscape, which then are cast into HA creating a secondary inverse mold. POC prepolymer/HA constructs are cured, and a resulting 3D POC scaffold is analyzed by micro-CT for its porosities and defects.[5,16,25] [Color figure can be viewed in the online issue, which is available at www.interscience.wiley.com.]

applied to delineate the solid POC material using GEMS MicroView software (GE Medical Systems, Toronto, CAN). All porosity scanning was performed before mechanical tests to avoid any artifacts due to compression. Also, any possible residuals of HA were checked by μCT images by applying a threshold level of HA. The intensity threshold of POC is -510 and that of HA is 2000–2500 at gray-scale values of Micro-CT images viewed by GEHC MicroView. By applying different threshold values, any HA residual within the POC scaffold can be determined.

Scaffold permeability ($N = 7$, each design) with and without composite hyaluronic acid (HyA)/collagen I (Col I) gel was measured using a previously built flow chamber.[25] Permeability was calculated as average mass flow from Bernoulli's equation (with a frictional loss correctional term)[23] with Darcy's Law used to calculate permeability. Permeability of scaffolds with hydrogels was measured to mimic cell loading conditions *in vitro* or *in vivo*.

Chondrocytes were seeded into 3D scaffolds by first suspending the cells in media with composite HyA/Col I gels and then pushing the gel into the 3D scaffolds.[16] The gelation procedure is as follows: 625 μL of Col I (stock concentration: 6 mg/mL; BD Bioscience Discovery Labs, San Jose, CA) with 62.5 μL HyA [stock concentration: 3 mg/mL in 1.5*M* sodium chloride (NaCl), molecular weight 2.4–3 million Da; Hyalogic LLC, Edwardsville, KS] were well mixed. The pH of the HyA/Col I suspension was increased with the addition of 9 μL of 0.5*N* sodium hydroxide with 220 mg/mL sodium bicarbonate to initiate gelation. As soon as 0.5*N* sodium hydroxide is added to HyA/Col I gel mixture, gel contents were evenly resuspended. Hydrogel mixtures were then dripped down onto preprepared sterile POC scaffolds until POC scaffolds were fully soaked and filled with gels up to the top surface. This was followed by incubation at 37°C for 30 min to solidify gels further. The gel mixture volumes used for each design varied depending on porosity of each design. Roughly, 90, 110, and 150 μL of gel mixtures were used for 32, 44, and 62% porous scaffolds, respectively. The permeabilities are presented as mean ± standard deviation.

In Vitro Scaffold Degradation

Four solid cylinders and four porous scaffolds (6.35 mm in diameter, 4.0–4.3 mm thickness) for each design were placed in a tube containing 10 mL phosphate buffer saline (PBS) (pH 7.4) for 3 weeks. Additionally, nine porous scaffolds for each design were degraded by 0.1*M* NaOH for 9, 24, and 33 h at 37°C to rapidly obtain relative degradation rates among samples. After incubation, samples were washed with water and oven-dried at 50°C for 24 h. Mass loss was calculated by comparing the initial mass (W_0) with the mass measured at a given time point (W_t), as shown in the following equation: Mass loss $= [(W_0 - W_t)/W_0]*100\%$. The results are presented as means ± standard deviation. For NaOH degradation, four 62% porous scaffolds were mechanically tested before and after degradation.[2,3,5]

In Vitro Cell Culture and Histology

Porcine chondrocytes (pChon) were isolated and seeded onto scaffolds following the methods previously published[16] with some modifications. In short, cells were resuspended at a density of 35×10^6 cells/mL in 625 μL of composite HyA/Col I with approximately 60 μL of culture medium. Collagen gels are used as a cell carrier for POC scaffolds to provide better cell distribution within scaffold pores. Five percent hyaluronic acids was added to provide a favorable environment for chondrocyte differentiation/proliferation based on our previous work.[16] The remaining steps were the same as previously described (see "Porosity and Permeability Measurements" section). Scaffolds seeded with pChon were cultured with chondrogenic medium [basal medium (DMEM), 10% fetal bovine serum (FBS), 1% P/S (Gibco) supplemented with 50 mg/mL 2-phospho-L-ascorbic acid (Sigma), 0.4 m*M* proline (Sigma), 5 mg/mL insulin (Gibco), and 0.1 m*M* nonessential amino acids (Gibco)]. Chondrocytes on scaffolds were cultured for 4 weeks under gentle agitation on an orbital shaker, and the media was changed every other day. All polymer samples were sterilized by incubation in 70% ethanol for 30 min, followed by UV light exposure for another 15 min each side before plating cells. After sterilization, all scaffolds were briefly rinsed with PBS, followed by soaking in basal medium to neutralize. Cell culture was maintained in a water-jacket incubator equilibrated with 5% CO_2 at 37°C for 4 weeks. For histology, constructs were fixed in 10% buffered formalin overnight, dehydrated with a series of graded ethanol, and embedded in paraffin. Tissue sections were stained with safranin-O (saf-O) to assess cell distribution, morphology, and sGAG staining as a measure for cartilage application. Three slides (4 sections/slide) were obtained from the center of each scaffold (top to bottom and left to right).

Statistical Analysis

Data are expressed as mean ± standard deviation. The statistical significance among different porosities was calculated using linear regressions and one-way ANOVA with post hoc comparison (Tukey). Data were taken to be significant when a p value of 0.05 or less was obtained.

RESULTS

Mechanical Tests

Figure 3(A) shows that unconfined compressive tests of POC solid and scaffolds produced stress–strain curves characteristic of elastomeric materials. As porosity of scaffolds increased, tangent moduli decreased. Solid and 32% porous scaffolds exhibited nonlinear behavior with increased strain level whereas 44 and 62% porous scaffolds were more lin-

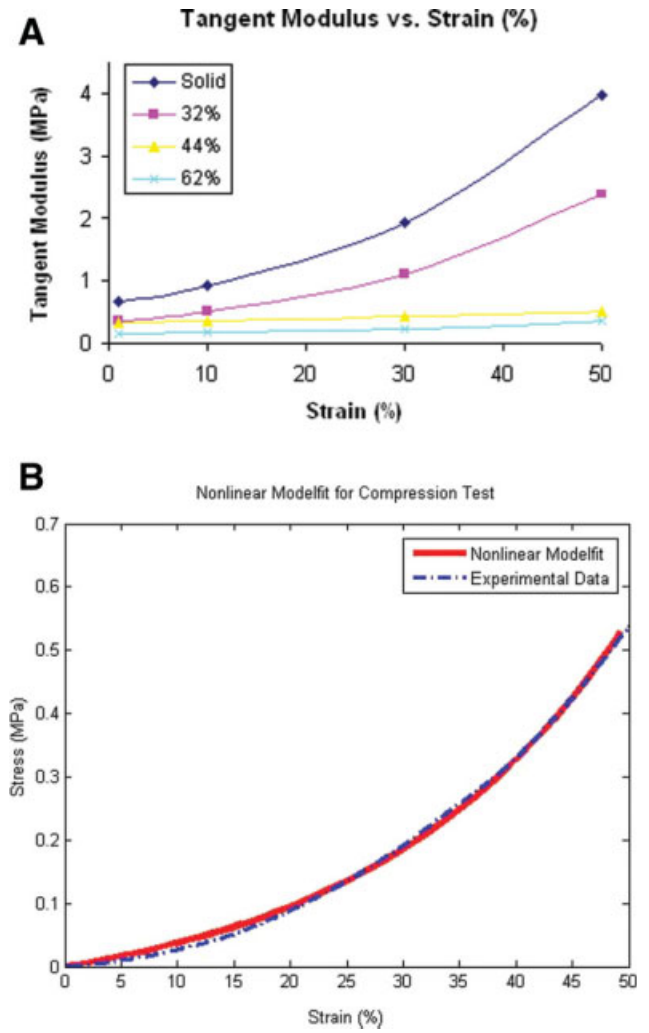

Figure 3. (A) A tangent moduli (MPa) versus strain (%) curve from unconfined compression tests and nonlinear model fit ($N = 7$, $p < 0.05$ for all porosities). (B) An example of compressive test data and corresponding nonlinear model fit for a 44% porous scaffold. [Color figure can be viewed in the online issue, which is available at www.interscience.wiley.com.]

ear. Figure 3(B) is an example of nonlinear model fit for a 44% porous scaffold and Table I summarizes tangent moduli for each design at various strain levels (%).

In cartilage engineering, many researchers have tried to design and fabricate scaffolds with stress–relaxation properties, mimicking the poroelastic biomechanics of cartilage. To determine if POC solid cylinders or scaffolds were also either viscoelastic or poroelastic, we have performed confined compressive tests as described earlier.[19–21] Results of stress–relaxation tests demonstrated that POC does not exhibit significant stress relaxation and thus can be considered as a nonlinear elastic material and not viscoelastic. Porous scaffolds also did not demonstrate stress relaxation, indicating that pores of the designed size did not exhibit poroelastic behavior.

Tensile test data for solid coupons exhibited nonlinear elastic behavior and was fit well with the Neohookean model (Figure 4). The coefficients differed with synthesis conditions, with 1 day of curing at 100°C followed by 4 days at 120°C giving a μ_1 value of 0.172 ± 0.022 MPa while 5 days of 100°C giving a μ_1 value of 0.142 ± 0.013 MPa. The coefficient of determination for all fits was greater than 0.99, indicating good fits for the nonlinear model.[26] In addition, all coefficients satisfied the Baker–Eriksen criteria for material stability. This demonstrates higher curing temperature gives an overall stiffer behavior for solid POC. These results also demonstrate that POC can be considered as a nonlinear elastic elastomeric material.

The major difference between linear and nonlinear elasticity is that, in linear elasticity, the material modulus is constant over the entire deformation, whereas for nonlinear elasticity, the modulus will change with deformation. In general, soft tissues, including cartilage, are shown to exhibit strain stiffening in which the tangent modulus increases with increasing strain.[26,33] If we accept the fact that mechanical strain magnitude can affect tissue regeneration in that cells may modulate matrix synthesis in response to strain levels, matching only the linear versus nonlinear behavior could have significant consequences for tissue regeneration. If only a material exhibiting linear behavior is used for a scaffold, we are faced with the choice of matching either the low modulus under small strains or the higher modulus under large strains. Matching the small-strain, low modulus may provide sufficient strain to stimulate cells under small deformation, but if large deformations are seen, then the cells may be damaged. If we match the large deformation higher modulus with a linear scaffold, this may protect the chondrocytes under large strain, but may shield the chondrocytes for sufficient mechanical stimulus under small strain. A nonlinear material that can match both regions may provide better strain microenvironments to chondrocytes. Of

TABLE I. Tangent Moduli (MPa) of Scaffolds at Various Strain (%) Presented as Average ± Standard Deviation and Average Model Fit Error (fval)

	Design (Porosity)				
Strain (%)	Solid[a]	32%[b]	44%[c]	62%[d]	Average fval
1	0.674 ± 0.147	0.372 ± 0.048	0.327 ± 0.046	0.147 ± 0.046	0.0064
10	0.933 ± 0.209	0.523 ± 0.061	0.355 ± 0.037	0.170 ± 0.052	0.0015
30	1.922 ± 0.475	1.115 ± 0.123	0.427 ± 0.035	0.244 ± 0.089	0.0023
50	3.977 ± 1.113	2.392 ± 0.343	0.519 ± 0.082	0.365 ± 0.182	0.0010

[a–d] $N = 7$ and $p < 0.05$.

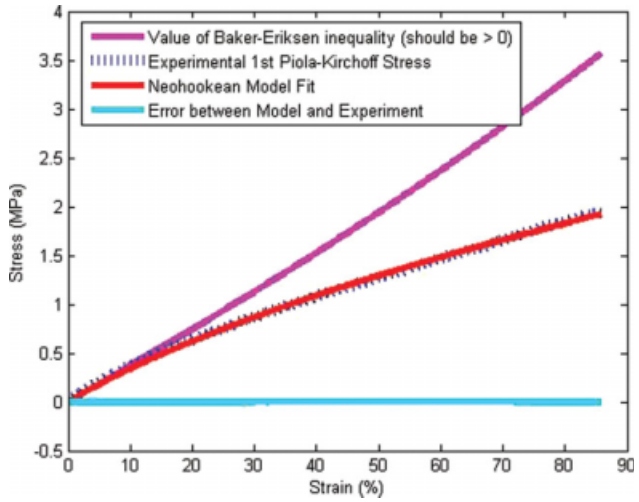

Figure 4. An example of tensile test data and corresponding Neohookean model fit. [Color figure can be viewed in the online issue, which is available at www.interscience.wiley.com.]

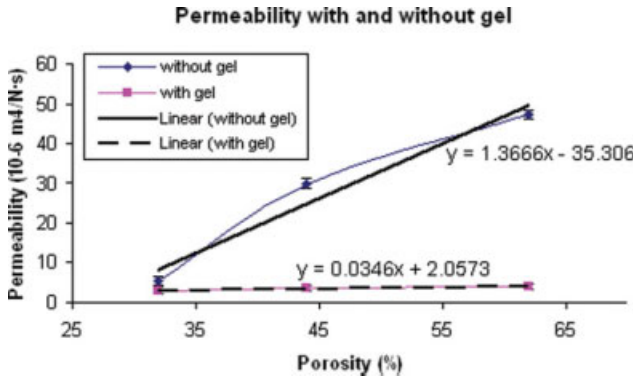

Figure 5. POC scaffold permeability with and without gel for different porosity ($N = 7$, $p < 0.05$). [Color figure can be viewed in the online issue, which is available at www.interscience.wiley.com.]

course, this is currently conjecture, but such hypotheses can only be tested if we can engineer scaffolds with both linear and nonlinear elastic behavior.

Based on previous reports,[27–32] aggregate modulus of human articular cartilage ranges from 0.1 to 3.10 MPa and unconfined compressive modulus ranges from 0.45 to 0.9 MPa with 10–30% strain, depending on ages and health conditions. POC scaffold tangent moduli range from 0.1 MPa (62% porosity at 1% strain) to 1.115 MPa (33% porosity at 30% strain). Thus, POC tangent moduli encompass the range of human articular equilibrium moduli.

Permeability

Table II shows permeability of scaffolds without and with hydrogels for various porosities. Generally, it is known that an increase in interconnected porosity results in an increase in permeability. However, permeability depends not only on scaffold architecture, but also on base materials because of the presence of micropores, hydrophilicity, and number of crosslinkages. Without gels, permeability increased dramatically with a linear regression coefficient of 0.1524, whereas permeability did not vary substantially between different designs with gel, having a linear regression coefficient of 0.0032 (Figure 5). The differences in permeability between cases with and without gel become more critical when cells are seeded onto scaffolds for tissue ingrowth. Even though scaffold architectures may have significantly different permeabilities, the use of gels for scaffold cell seeding may temporarily cause a significant drop in permeability. However, the relatively quick hydrogel degradation will cause a steady increase in scaffold permeability.

TABLE II. Permeability of Scaffold Designs with and Without Collagen I Gel ($N = 7$, $p < 0.05$ for Both with and Without Gel)

	Permeability (10^{-6} m^4/N·s)		
Porosity (%)	32	44	62
Without gel	0.54 ± 0.12	2.98 ± 0.21	5.24 ± 0.89
With gel	0.31 ± 0.04	0.37 ± 0.03	0.41 ± 0.07

In Vitro Degradation

Yang et al.[3] demonstrated that the degradation rate could be adjusted by varying synthesis and fabrication conditions of POC solids. They demonstrated that increased curing temperature and postpolymerization time resulted in a higher tensile strength and a higher Young's modulus due to higher crosslink density and fewer unreacted monomer groups, but those synthesis conditions tend to make a material that degrades slower. However, they did not investigate how different scaffold architectures could affect POC degradation and associated changes in compressive mechanical properties. The data for degradation of POC scaffolds with various porosities are presented in Figure 6. Both fast (0.1*M* NaOH) and slow (PBS) degradation showed a similar trend in terms of different degradation profiles for each design.

Degradation, perhaps due to both bulk and surface erosion, was highly dependent on scaffold porosity and permeability (Figure 6). Both the 32 and 44% scaffolds showed loss of architecture and complete pore collapse after 3-week degradation in PBS. All designs showed loss of architecture after 24 h in 0.1*M* NaOH. A significant portion of the 62% porous scaffold showed pore collapse, although the top layer of the scaffold maintained the pore structure. Based on these results, it is not possible to make a definitive conclusion as to the mechanism of degradation, bulk versus surface. The nature of the pore collapse suggests that both mechanisms may be involved.

In this study, the lower porosity scaffolds with thicker struts showed a greater degree of collapse than the 62% porous scaffolds with the thinnest struts. If the sole mechanism of degradation was surface erosion, one would expect that the 62% porous scaffold with the thinnest struts would collapse sooner, as the struts would lose thickness and geometry first. However, the thinnest struts did not collapse first, suggesting that bulk degradation with autocatalysis could play a role in POC porous architecture degradation.

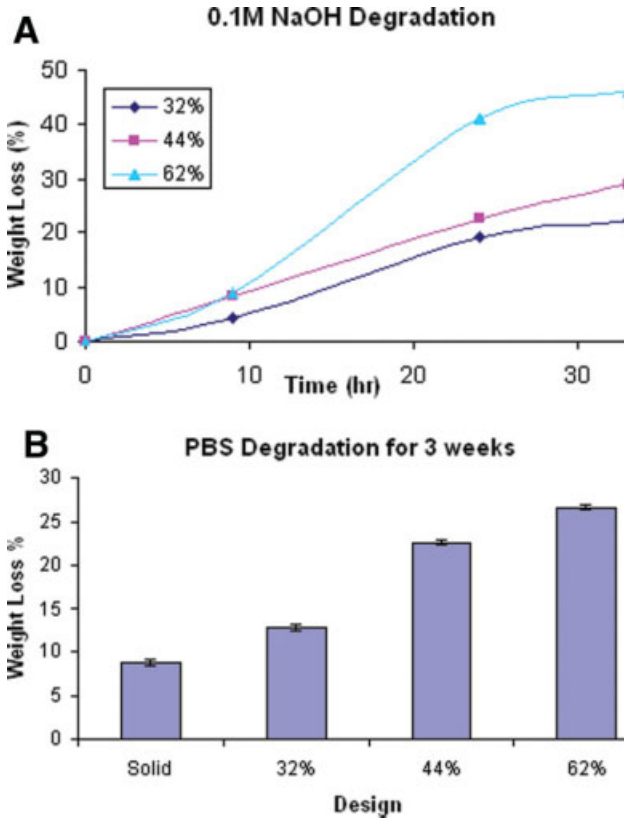

Figure 6. Degradation studies of POC scaffolds with various porosities in (A) 0.1*M* NaOH solution at room temperature ($N = 9$, each porosity) ($p < 0.05$) and (B) PBS at 37°C ($N = 4$, each porosity) ($p < 0.05$). [Color figure can be viewed in the online issue, which is available at www.interscience.wiley.com.]

Tangent Young's modulus (10–20% strain range) for 62% scaffolds decreased from 0.070 to 0.037 MPa after PBS degradation. In Figure 6(A), initial degradation rate did not seem to vary much depending on different porosities; however, permeability effects were associated with higher degradation rates at longer time periods as determined by weight loss.

Biocompatibility Evaluation

Cartilaginouslike tissue was formed within POC scaffolds and chondrocytes in lacuna were evenly distributed within the tissue. These cells maintained a rounded form, indicating maintenance of the chondrocytes phenotype [Figure 7(B)]. The void spaces shown in Figure 7(a, b) are areas occupied by POC scaffolds. The chondrocytic morphology and tissue formation confirm the biocompatibility of the POC scaffolds.

DISCUSSION

The success in development of novel biodegradable polymers for scaffolds relies on appropriate mechanical properties, degradation rates, and biocompatibility. It is critical to understand how scaffold architectures affect mechanical, mass transport, and degradation properties of scaffolds as these properties will significantly influence tissue regeneration. A typical solid elastomer shows a nonlinear behavior in compression and tension.[3] However, the degree of nonlinearity in compression depended significantly on scaffold porosity. As porosity increased, nonlinear behavior decreased and 44 and 62% porous scaffolds had a trend toward more linear behavior. Because of the inherent POC nonlinear behavior, solid and 32% porous scaffolds showed a distinct increase in compressive tangent moduli compared with higher porosities.

Permeability showed a more complex relationship to scaffold architecture, depending on the presence or absence of gel cell carriers. Scaffold permeability without gel showed a linear relationship with porosity (Figure 5). Based on permeability without gel, we may deduce that water could penetrate through both gel and POC itself at similar rates because the regression coefficients did not depend significantly on porosity when the scaffold contained gel. This data are especially important when consid-

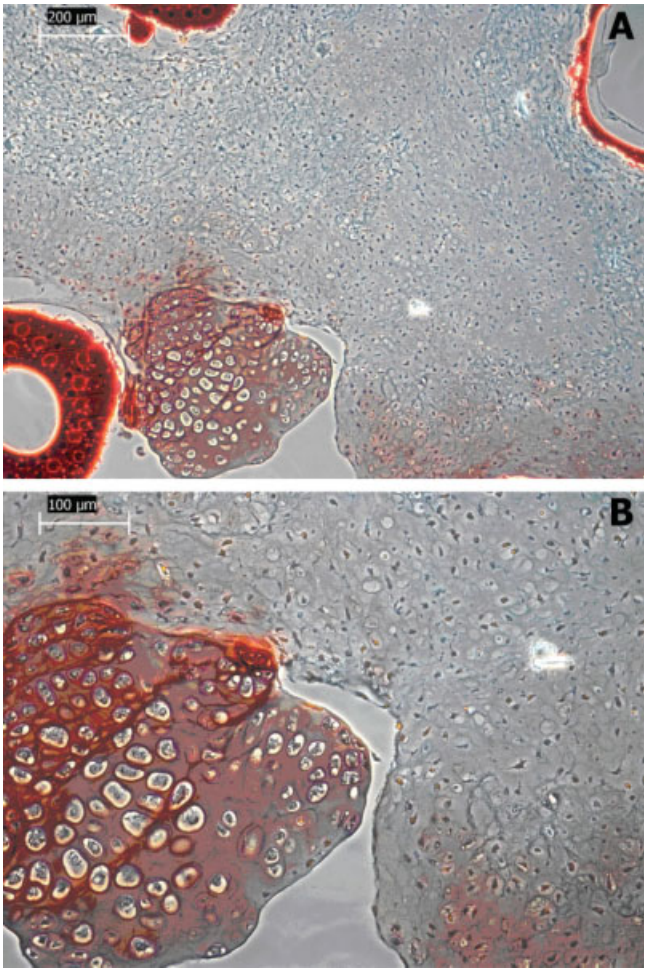

Figure 7. (A and B) Histological studies of POC scaffolds with chondrocytes for 4 weeks. The sections were stained with safranin O. Stars indicate areas occupied by scaffold materials. [Color figure can be viewed in the online issue, which is available at www.interscience.wiley.com.]

ering seeding cells with gels onto POC scaffolds. The degradation rates were also highly dependent on porosity and permeability. Sixty-two percent porous scaffolds exhibited faster and accelerated degradation rates with time, whereas 32 and 44% porous scaffolds showed a steady linear increase in degradation rates with time [Figure 6(A)]. Data for degradation with PBS for 3 week showed an interesting phenomenon in that only 62% porous scaffolds maintained some porous architecture at 3-week time point while other designs all exhibited distorted inner architectures due to degradation. When measured compressive modulus, Young's modulus was decreased by up to 47%.

In vitro histological evaluation of POC scaffolds with gel confirmed that they supported synthesis of cartilage matrix by chondrocytes. Also, chondrocytic morphology of scaffold was also maintained, showing its promising potential as a scaffold for cartilage regeneration.

The above characterization provides us with a comprehensive understanding of the physical properties of POC scaffolds. POC scaffolds hold promise for serving as a supporting template for cartilage and other soft tissue regeneration with tunable biodegradation and nonlinear compliant mechanical properties. Also, this characterization provides us with a foundation to study cell behavior and tissue ingrowth on different scaffold architectures to elucidate the relation between scaffold architectures, mechanical properties, biodegradation, and consequent cell growth and morphology.

CONCLUSION

Poly(1,8 octanediol-*co*-citrate) scaffolds exhibit controllable biodegradation and nonlinear mechanical properties that are suitable for cartilage and other soft tissue regeneration. Increasing porosity decreases stiffness and the degree of nonlinear behavior, but increases permeability and degradation rate of POC scaffolds. Thus, when designing scaffolds for soft tissue application, the trade off between effective scaffold mechanical, mass transport, and degradation behavior resulting from designed porosity should be taken into account. The characterization of 3D POC scaffolds and the relation between scaffold architectures and mechanical properties provide a basic foundation for determining how scaffold architecture affects tissue regeneration. The detailed characterization of mechanical and mass transport properties should expand and elucidate the potentials of POC as a soft tissue scaffold.

The authors thank Alisha Diggs and Eiji Saito for help with HA mold fabrication, Jessica M. Kemppainen for help with permeability measurements, and Chris Strayhorn for assistance with histology.

REFERENCES

1. Safran MR, Kim H, Zaffagnini S. The use of scaffolds in the management of articular cartilage injury. J Am Acad Orthop Surg 2008;16:306–311.
2. Yang J, Webb AR, Ameer GA. Novel citric acid-based biodegradable elastomers for tissue engineering. Adv Mater 2004;16:511–516.
3. Yang J, Webb AR, Pickerill SJ, Hageman G, Ameer GA. Synthesis and evaluation of poly(diol citrate) biodegradable elastomers. Biomaterials 2006;27:1889–1898.
4. Hidalgo-Bastida LA, Barry JJ, Everitt NM, Rose FR, Buttery LD, Hall IP, Claycomb WC, Shakesheff KM. Cell adhesion and mechanical properties of a flexible scaffold for cardiac tissue engineering. Acta Biomater 2007;3:457–462.
5. Kim K, Jeong CG, Hollister SJ. Non-invasive monitoring of tissue scaffold degradation using ultrasound elasticity imaging. Acta Biomater 2008;4:783–790.
6. Wang Y, Ameer GA, Sheppard BJ, Langer R. A tough biodegradable elastomer. Nat Biotechnol 2002;20:602–606.
7. Motlagh D, Yang J, Lui KY, Webb AR, Ameer GA. Hemocompatibility evaluation of poly(glycerol-sebacate) in vitro for vascular tissue engineering. Biomaterials 2006;27:4315–4324.
8. Sundback CA, Shyu JY, Wang Y, Faquin WC, Langer RS, Vacanti JP, Hadlock TA. Biocompatibility analysis of poly-(glycerol sebacate) as a nerve guide material. Biomaterials 2005;26:5454–5464.
9. Gao J, Ensley AE, Nerem RM, Wang Y. Poly(glycerol sebacate) supports the proliferation and phenotypic protein expression of primary baboon vascular cells. J Biomed Mater Res A 2007;83:1070–1075.
10. Gao J, Crapo PM, Wang Y. Macroporous elastomeric scaffolds with extensive micropores for soft tissue engineering. Tissue Eng 2006;12:917–925.
11. Chen QZ, Bismarck A, Hansen U, Junaid S, Tran MQ, Harding SE, Ali NN, Boccaccini AR. Characterisation of a soft elastomer poly(glycerol sebacate) designed to match the mechanical properties of myocardial tissue. Biomaterials 2008;29:47–57.
12. Wang S, Kempen DH, Simha NK, Lewis JL, Windebank AJ, Yaszemski MJ, Lu L. Photo-cross-linked hybrid polymer networks consisting of poly(propylene fumarate) and poly(caprolactone fumarate): Controlled physical properties and regulated bone and nerve cell responses. Biomacromolecules 2008;9:1229–1241.
13. Kang Y, Yang J, Khan S, Anissian L, Ameer GA. A new biodegradable polyester elastomer for cartilage tissue engineering. J Biomed Mater Res A 2006;77:331–339.
14. Hollister SJ, Maddox RD, Taboas JM. Optimal design and fabrication of scaffolds to mimic tissue properties and satisfy biological constraints. Biomaterials 2002;23:4095–4103.
15. Hollister SJ. Porous scaffold design for tissue engineering. Nat Mater 2005;4:518–524.
16. Liao E, Yaszemski M, Krebsbach P, Hollister S. Tissue-engineered cartilage constructs using composite hyaluronic acid/collagen I hydrogels and designed poly(propylene fumarate) scaffolds. Tissue Eng 2007;13:537–550.
17. Taboas JM, Maddox RD, Krebsbach PH, Hollister SJ. Indirect solid free form fabrication of local and global porous, biomimetic and composite 3D polymer-ceramic scaffolds. Biomaterials 2003;24:181–194.
18. Kemppainen JM, Hollister SJ. Tailoring the mechanical properties of 3D-designed poly(glycerol sebacate) scaffolds for cartilage applications. J Biomed Mat Res. Forthcoming.
19. Ateshian GA, Warden WH, Kim JJ, Grelsamer RP, Mow VC. Finite deformation biphasic material properties of bovine articular cartilage from confined compression experiments. J Biomech 1997;30:1157–1164.
20. Soltz MA, Ateshian GA. Experimental verification and theoretical prediction of cartilage interstitial fluid pressurization at an impermeable contact interface in confined compression. J Biomech 1998;31:927–934.

21. Soltz MA, Ateshian GA. Interstitial fluid pressurization during confined compression cyclical loading of articular cartilage. Ann Biomed Eng 2000;28:150–159.
22. Guilak F, Best BA, Ratcliffe A, Mow VC. Instrumentation for load and displacement controlled studies on soft connective tissues. AMD 1989;98:113–116.
23. Hollister SJ, Liao EE, Moffitt EN, Jeong CG, Kemppainen JM. Defining design targets for tissue engineering scaffolds. In: Meyer U, editor. Fundamentals of Tissue Engineering and Regenerative Medicine. Berlin: Springer-Verlag, 2009.
24. Holzapfel GA. Nonlinear Solid Mechanics: A Continuum Approach for Engineering. Wiley; 1st Edition. 2000;235–239.
25. Kemppainen JM. Mechanically stable solid freeform fabricated scaffolds with permeability optimized for cartilage tissue engineering. Ph.D. dissertation, University of Michigan, Ann Arbor, MI, 2008.
26. Humphrey JD. Cardiovasc Solid Mech 2002;198–201.
27. Demarteau O, Wendt D, Braccini A, Jakob M, Schafer D, Heberer M, Martin I. Dynamic compression of cartilage constructs engineered from expanded human articular chondrocytes. Biochem Biophys Res Commun 2003;310:580–588.
28. Boschetti F, Pennati G, Gervaso F, Peretti GM, Dubini G. Biomechanical properties of human articular cartilage under compressive loads. Biorheology 2004;41:159–166.
29. Huang CY, Mow VC, Ateshian GA. The role of flow-independent viscoelasticity in the biphasic tensile and compressive responses of articular cartilage. J Biomech Eng 2001;123: 410–417.
30. Armstrong CG, Mow VC. Variations in the intrinsic mechanical properties of human articular cartilage with age, degeneration, and water content. J Bone Joint Surg Am 1982;64:88–94.
31. Armstrong CG, Mow VC. The mechanical properties of articular cartilage. Bull Hosp Jt Dis Orthop Inst 1983;43: 109–117.
32. Mansour JM. Biomechanical Principles (Part I): Biomechanics of Cartilage. In: Oatis CA, editor. Philadelphia: Lippincott Williams and Wilkins; 2003 Ch. 5. 68–77.
33. Nugent GE, Schmidt TA, Schumacher BL, Voegtline MS, Bae WC, Jadin KD, Sah RL. Static and dynamic compression regulate cartilage metabolism of PRoteoGlycan 4 (PRG4). Biorheology 2006;43:191–200.